TECHNICAL FEATURE

DEVELOPMENT OF AN ADVANCED AIRBORNE PRECIPITATION RADAR

Radar has been used for observation of weather since the 1940s.[1] Advances in weather radar include the incorporation of Doppler capability, which allows measurement of wind velocity, and the use of multiple polarizations, which enhance rainfall estimation and provide the ability to discriminate between types of hydrometeors, such as hail versus rain. The first spaceborne weather radar was launched in 1997. The Tropical Rainfall Measuring Mission (TRMM) payload includes a 14 GHz precipitation radar (PR), which can provide estimates of rainfall as a function of altitude within its 220 km swath.[2] In response to TRMM's success, various potential improvements to the PR have been considered for future spaceborne weather radars. Key improvements include the use of Doppler[3] and dual-polarization, real-time pulse compression for improved sensitivity, dual-frequency operation for improved rainfall retrieval,[4,5] enhanced swath and reduced mass.

As part of a recent study, a complete spaceborne second generation precipitation radar (PR-2) has been designed.[6] This new system will offer greatly enhanced capability with much smaller mass than the TRMM PR. The PR-2 operates at 13.4 GHz (Ku-band) and 35.6 GHz (Ka-band), and uses a deployable 5.3 m electronically-scanned membrane antenna. The operating frequencies were chosen to be within the current allocation for spaceborne radar remote sensing. The antenna is a cylindrical parabolic reflector with a linear phased array feed. This allows cross-track scanning out to at least 30° from nadir, more than doubling the swath width relative to the TRMM PR. The antenna is designed to have low side lobes (near –30 dB) to minimize surface clutter when scanned away from nadir.

To demonstrate the PR-2 design, an airborne prototype (the Airborne PR-2 or APR-2) has been developed and flown on the NASA DC-8 aircraft. APR-2 uses the PR-2 design for its digital and lower frequency RF subsystems. In place of the large 5.3 m active antenna for the spaceborne PR-2, a mechanically-scanned antenna and traveling wave tube amplifiers are used for the APR-2.

Fig. 1 APR-2 operational geometry.

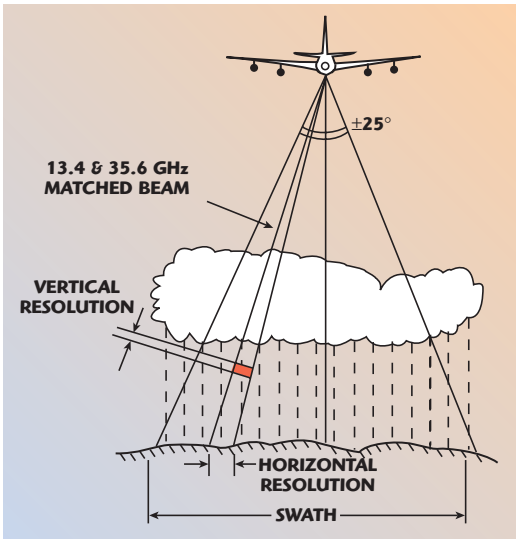

DESIGN CONSIDERATIONS

Figure 1 shows the operational geometry of APR-2. The DC-8 aircraft is flying out of the page, and the antenna scan in the cross-track is in the plane of the page. This scanning geometry is essentially the same as that for both the TRMM PR and the spaceborne PR-2. In designing APR-2, a number of tradeoffs were considered. For a given antenna size, a higher operating frequency results in greater received power backscattered from weather targets. However, for dual-frequency retrievals of rainfall, it is desirable that the antenna beams be matched as closely as possible at the two frequencies. Hence, both the airborne and spaceborne versions of PR-2 have matched beams. Another tradeoff is received power versus range resolution. For distributed targets such as precipitation, the radar equation shows that the re-

G.A. SADOWY, A.C. BERKUN, W. CHUN, E. IM AND S.L. DURDEN
Jet Propulsion Laboratory,
California Institute of Technology
Pasadena, CA

ceived power is proportional to the length of the transmit pulse.[7] For conventional short pulse operation, as is used in the TRMM PR, the range resolution also directly depends on the pulse length. An alternative is pulse compression,[8] which allows use of a long pulse to improve sensitivity but provides range resolution that depends on the signal bandwidth rather than pulse length. To achieve this resolution, the received signal is correlated with a replica of the transmitted signal. This results in most of the signal energy being concentrated in a narrow main lobe with width determined by the bandwidth. Due to the finite nature of the signal, some energy ends up in range side lobes, rather than the main lobe. There are at least two challenges that must be met to make pulse compression practical for a downward-looking precipitation radar.

The first challenge results from the surface being much more reflective than the rain above it. Hence, it is quite possible for range side lobes from the surface to obscure the return from rain just above the surface. To avoid this situation, it is necessary that pulse compression side lobes relative to the peak correlation be near –60 dB or lower[9] at Ku-band and near –50 dB at Ka-band. Several pulse compression waveforms were studied, including linear and nonlinear frequency modulation (FM), and binary coding. A linear FM chirp waveform with amplitude weighting was chosen to minimize sensitivity of the range side lobe level to Doppler shifting of the received signal. Gain and phase errors in the system must be kept to a minimum to avoid increased pulse compression side lobes.[8] The same technique was used on a previous airborne system which achieved side lobes near –60 dB.[10] On that system all pulses were recorded on a high speed tape recorder and processed on the ground. Such an approach is not practical in space, so a real-time solution is the second challenge presented by using pulse compression. To achieve low side lobes, digital processing is needed. After studying a variety of options, including general purpose computers and digital signal processors, a solution using field programmable gate arrays (FPGA) was developed, the details of which are described in the next section. This approach uses a time domain pulse compression algorithm, which can be implemented as a digital filter.

Several other system level design considerations were studied. At least 64 independent samples must be averaged to reduce signal fading to acceptable levels for rainfall retrieval, as is done for the TRMM PR. This requires appropriate choices of system timing and antenna scan rate. The pulse repetition frequency (PRF) is chosen to be near 5000 Hz to provide high correlation between pulses, pro-

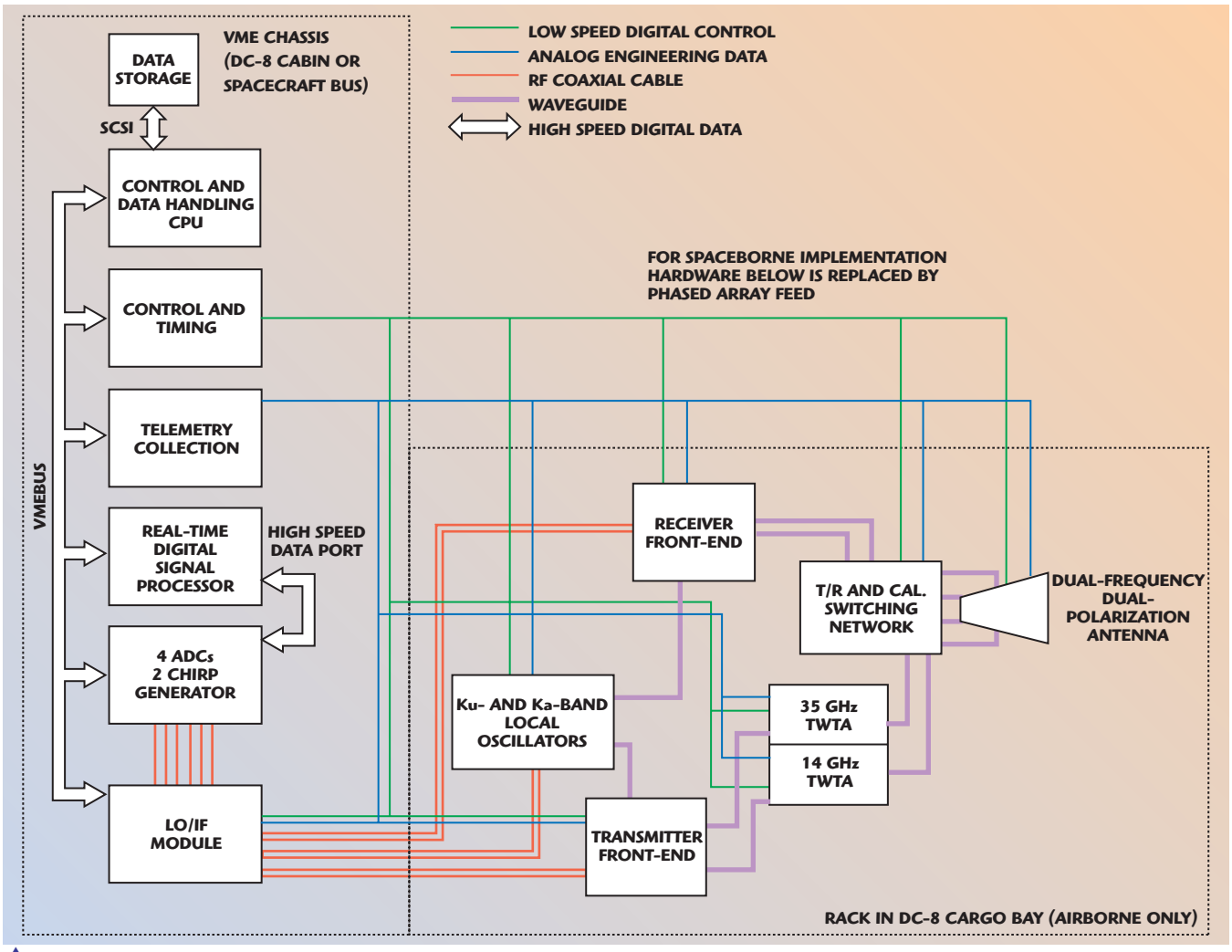

Fig. 2 Block diagram of APR-2 subsystems.

viding better than 1 m/s precision on the Doppler velocity estimate.[7,9] Accurate Doppler also puts a requirement on the frequency stability or phase noise in the system.[7] Finally, acquisition of both co-polarized and cross-polarized signals in APR-2 enhances discrimination between ice and water,[7,9] requiring sufficient isolation between the co-polarized and cross-polarized channels.

SYSTEM DESCRIPTION

The APR-2 is implemented to demonstrate as much of the spaceborne radar technology as possible, while making use of a mechanically-scanned passive antenna for airborne operation. The APR-2 thus couples spaceflight-like digital electronics and lower frequency RF electronics with airborne-specific high frequency electronics and traveling wave tube amplifiers (TWTA). A 6U VME form factor was chosen for the digital electronics boards. The local oscillator and intermediate frequency (LO/IF) module was also constructed to fit within two slots in the same VME cage, providing an extremely compact implementation that is suitable for spaceborne operation. In a spaceborne implementation the same digital electronics and LO/IF module would be coupled with an active electronically-scanned antenna and associated electronics for up conversion and down conversion. ***Figure 2*** provides a block diagram of the APR-2 showing the various subsystems and assemblies, distinguishing between that part which would fly in space with the spaceborne PR-2 and the part that is specific to the airborne system.

The radar operation can be described by tracing a pulse through the transmit and receive chains. The digital electronics generate linear FM chirps, which are passed to the RF electronics. The lower frequency (below 1.5 GHz) RF circuitry is all contained in the LO/IF module. This unit converts transmit chirp signals from 15 MHz up to 1405 MHz and down converts received IF signals from 1405 to 5 MHz. It also generates local oscillators at 40, 1350 and 1360 MHz, and provides the 10 MHz system master oscillator (MO). All other oscillators as well as the data system are locked to the 10 MHz MO, as required for pulse-to-pulse coherence. ***Figure 3*** shows a block diagram of one of the LO/IF channels. Programmable attenuators are provided to reduce the received signal level at the analog-to-digital converters (ADC) from strongly reflecting targets.

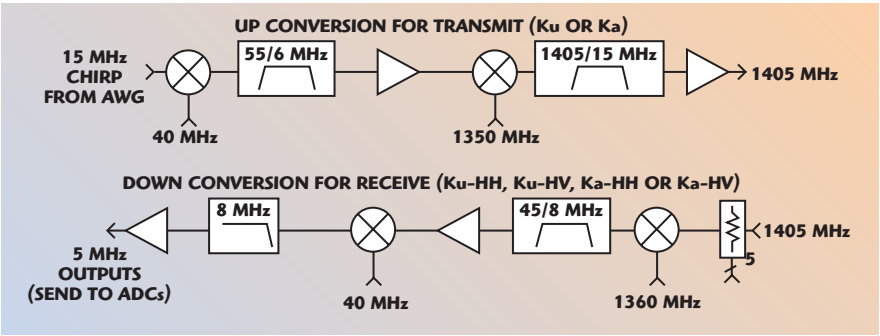

▲ *Fig. 3 Block diagram of one of the channels in the LO/IF module.*

Fig. 4 Block diagram of one of the local oscillators and up converters, and one of the four receiver channels. ▼

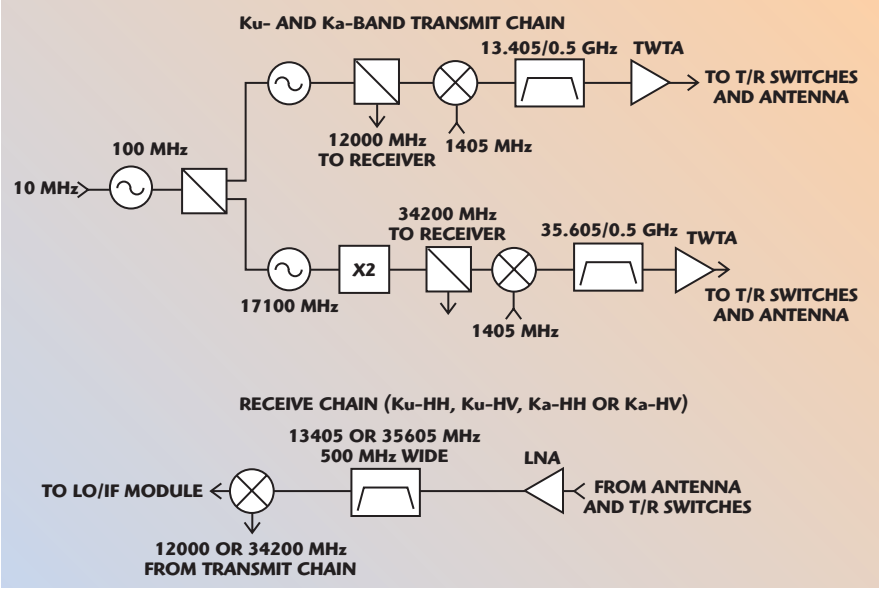

Figure 4 shows a block diagram of one of the local oscillators and up converters, and one of the four receiver channels.

The RF transmit front-end electronics for the APR-2 consists of five units: one local oscillator/ up converter (LO/U) unit; two TWTAs; and two waveguide front-end (WGFE) units. The LO/U receives two 1405 MHz IF chirp signals and a 10 MHz reference from the LO/IF. A 100 MHz crystal oscillator locked to the 10 MHz reference generates a signal that is used to phase lock two dielectric resonance oscillators operating at 12.0 and 17.1 GHz. The 12.0 LO is used for the first stage of up and down conversion for the Ku-band channels and the 17.1 GHz signal is doubled to yield a 34.2 GHz LO for the Ka-band channel. The 1405 MHz chirps are mixed with these local oscillator signals to yield chirps at 13.405 and 35.605 GHz. These signals are filtered, amplified and distributed to the inputs of the TWTAs, as shown in ***Figure 4***. The 12.0 and 34.2 GHz LO signals are also routed through waveguide to the two WGFEs where they are used in the first stage of receiver down conversion.

The WGFE units at each frequency contain transmit/receive (T/R) switches, calibration loops, low noise amplifiers (LNA) and the first-stage receiver mixers. During the transmit interval, the amplified chirp from the TWTA is routed to the antenna feed. A small sample of the transmit signal is coupled off and passed through a calibrated attenuator network. It is then coupled back into the receiver, which has both co-polarized and cross-polarized channels at each frequency. In the co-polarized (HH) channel, four circulators are used to isolate the receiver from the transmitter with the final one also being used to couple the calibration signal into the receiver. In the cross-polarization (HV) channel, only three are required

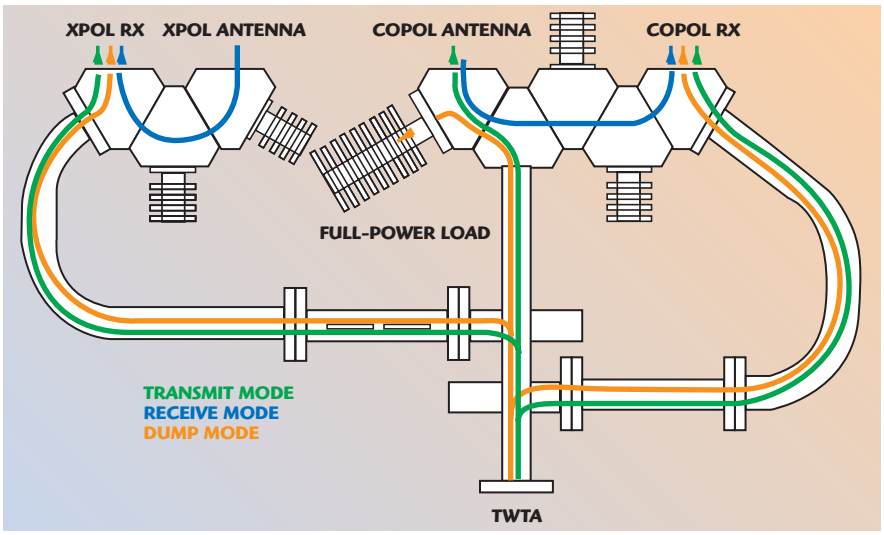

Fig. 5 Waveguide front-end signal routing.

because the antenna feed provides additional isolation. By measuring the power coupled into the receiver during the transmit interval, drifts in transmitter output power and receiver gain can be corrected. However, it is essential that unwanted leakage paths be suppressed so that they do not corrupt this power measurement. The calibration loop attenuation has been adjusted to place the calibration loop power near the top of the receiver's linear dynamic range, thereby maximizing the power ratio between the calibration signal and undesired leakages. For testing purposes, the transmit signals can also be routed to a load rather than the antenna. ***Figure 5*** shows the waveguide signal routing and front-end switches.

Signals from both TWTAs are sent to the 0.4 m diameter offset parabolic reflector antenna. This antenna was used in a previous single-frequency system.[10] The single-frequency feed horn is replaced by a dual-frequency feed horn, designed and fabricated by Microwave Engineering Corp. The feed includes an ortho-mode transducer to provide two orthogonal polarizations at each frequency. The signals are focused by the parabolic reflector and reflected to a flat mechanically-scanned elliptical reflector which scans the beam ±25° in the cross-track direction. The aperture at 35.6 GHz is under-illuminated to provide matched beams at the two frequencies.

During the receive interval, the signals from the antenna are routed directly to the two receiver inputs. Both co-polarized and cross-polarized signals are received at each frequency, for a total of four receive channels. LNAs are attached directly to the circulator networks in order to reduce the system noise. The outputs of the LNAs are bandpass filtered and routed to the first-stage mixers. After mixing down to 1405 MHz and filtering, the received signals are sent via coaxial cable to the LO/IF unit where further down conversion and filtering is performed. The LO/IF module outputs all four channels centered at a carrier frequency of 5 MHz and having 4 MHz bandwidth. These signals are digitized for further processing.

The digital electronics subsystem includes a control and timing unit (CTU), arbitrary waveform generators (AWG), ADCs for the four receiver channels, a data processor and a data formatter. The CTU decodes all radar mode commands and generates the required timing signals. It also controls the timing of the antenna beam scan. The transmit waveform is generated by a custom two-channel AWG which yields 14-bit resolution at a sample rate of 40 samples/s. Using AWGs instead of a traditional numerically controlled oscillator allows implementation of amplitude weighting of the pulse for sidelobe control.

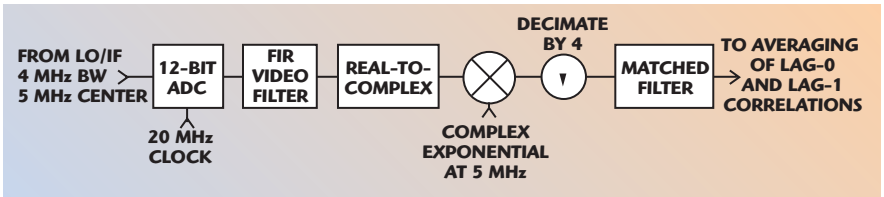

Fig. 6 Diagram of signal processing following digitization.

The real-time signal processor card is a VME card made by Annapolis Microsystems, with FPGA code developed by Andraka Consulting Group Inc. The board contains three large Xilinx Vertex FPGAs, reprogrammable parts that can be configured as almost any kind of digital logic. With four channels, the system performs 20 billion multiplications and 20 billion additions per second. This processing throughput would be difficult to achieve with general-purpose microprocessors. FPGAs enable implementation of efficient, algorithm-specific circuitry without the nonrecurring costs and development time associated with application-specific integrated circuits (ASIC).

The four receive channels are digitized by a custom 12-bit ADC board based on an Analog Devices 14-bit converter. ***Figure 6*** shows one of the four channels of the data processor. The front-end of the processor is four 64-tap, 16-bit finite impulse response (FIR) filters implemented with bit serial multipliers clocking at 133 MHz. The filter receives offset video sampled at 20 MHz and selects a 4 MHz flat bandwidth centered around 5 MHz, with 70 dB suppression of the 4 MHz band centered around DC. Following the filter, complex demodulation and decimation are performed, yielding in-phase and quadrature baseband signals. After demodulation, pulse compression is performed using a matched filter, realized as a 256-tap complex FIR filter loaded with a 12-bit reference function sampled at 5 MHz. The reference function is an ideal linear FM chirp with sinusoidal weighting on the first and last thirds and flat in the middle third. For every range sample the co- and cross-polarized echo power is computed. The pulse-pair technique[7] is used to calculate the Doppler velocity. Hence, the processor calculates the lag-0 correlation, or magnitude-squared of each sample, as well as the lag-1 correlation, that is, the correlation between successive pulses. The power and

pulse-pair estimates from up to 250 pulses are then averaged, yielding a 250-fold reduction in the output data rate. Any echo containing a saturated ADC value is dropped from the averages because even a single clipped ADC sample creates large range side lobes which can obscure much of the useful data near the ocean surface.

APR-2 is controlled by a VME-based computer, running the Unix operating system. Software, written in the C language, interfaces with the radar operator, loads the CTU and processor with the desired parameters, reads and stores data, and provides real-time display. APR-2 is mounted in the cargo bay of the NASA DC-8 aircraft. The antenna beam is directed through an opening in the bottom of the aircraft. A thin radome covers this observation port, and the entire antenna system is surrounded by a pressure box. The front-end RF electronics and TWTAs are located in the cargo bay near the pressure box. The LO/IF module, digital electronics and control computer are located in a rack in the passenger area.

APR-2 PERFORMANCE

Tests of APR-2 include laboratory measurements, engineering test flights off the California coast and science flights during the fourth Convection and Moisture Experiment (CAMEX 4) in Florida. This experiment had the goal of applying advanced remote sensing technology to study hurricanes. ***Table 1*** shows the performance characteristics of the APR-2 based on measurements. The horizontal resolution and ground swath reference to an aircraft altitude of 11 km. The minimum Z_e is the equivalent radar reflectivity factor in decibels relative to 1 mm^6/m^3 (dBZ); rain with this reflectivity would produce a signal roughly equal to the system thermal noise. Typically, 20 dBZ corresponds to light rain (1 to 2 mm/h) and 50 dBZ to very heavy rain. Reflectivity may reach 60 dBZ or more in hail. One of the key performance parameters requiring verification is the pulse compression side lobe level. This can be seen in ***Figure 7***, which is the APR-2 signal from the ocean surface in rain-free conditions. The range side lobes prior to the ocean are approximately –55 to –60 dB. For the receiver gain used at Ka-band, the side lobes are at roughly the same level as thermal and quantization noise. Such rain-free measurements were also used to verify the thermal noise performance and isolation between polarization channels. For a 10 µs chirp the minimum detectable reflectivity at 10 km range is roughly 13 dBZ at Ku-band and 10 dBZ at Ka-band. It is anticipated that these levels will be reduced in the future by improvements in the signal processor to enhance dynamic range. The cross-polarization response to the ocean at nadir is approximately –30 dB at Ku-band. Since the ocean cross-polarization backscatter at nadir is extremely low, it can be concluded that the system polarization isolation is approximately –30 dB at Ku-band. At Ka-band the isolation is no better than –20 dB; however, this does not impact the primary Ka-band measurement, which is the co-polarized reflectivity.

TABLE 1

PR-2 SYSTEM PARAMETERS

Frequency (GHz)	13.405	35.605
Polarization	HH,HV	HH,HV
Antenna effective diameter (m)	0.40	0.14
Antenna gain (dBi)	34	33
Antenna side lobe (dB)	–32	–37
Antenna beamwidth (°)	3.8	4.8
Peak power (W)	200	100
Bandwidth (MHz)	4	4
Pulsewidth (µs)	10 to 40	10 to 40
PRF (kHz)	5	5
Vertical resolution (6 dB) (m)	60	60
Horizontal resolution (6 dB) (m)	730	920
Ground swath width (km)	10	10
Z_e minimum at 10 km, 10 µs chirp (dBZ)	13	10
Doppler precision (m/s)	0.4	1.0

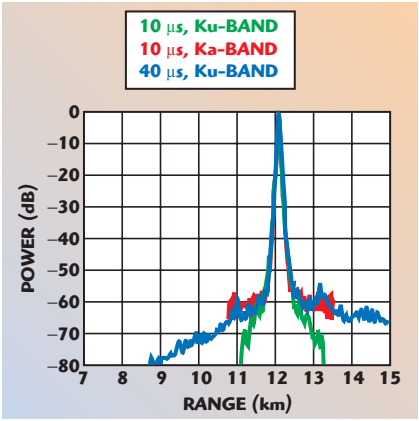

▲ *Fig. 7 Compressed pulses after reflection from the ocean surface in rain-free conditions.*

Fig. 8 Observed surface Ku-band Doppler vs. that predicted. ▼

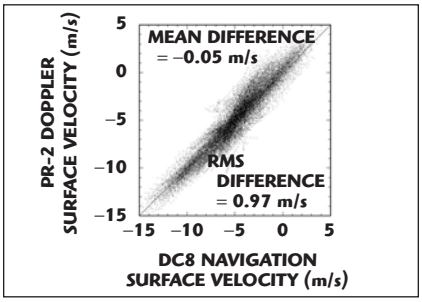

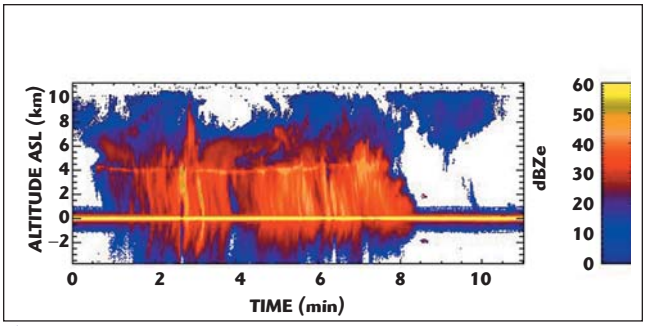

▲ *Fig. 9 Ku-band reflectivity in Hurricane Humberto along track.*

Figure 8 shows the observed PR-2 Ku-band Doppler, as compared with the Doppler predicted by using the aircraft navigation parameters. The measured Doppler is generally in very good agreement with the prediction, with a mean difference of only 0.05 m/s.

Figure 9 shows an image of Ku-band reflectivity in Hurricane Humberto on 25 September 2001. These data were acquired at nadir; the horizontal axis is time, or along-track distance, and the vertical axis is alti-

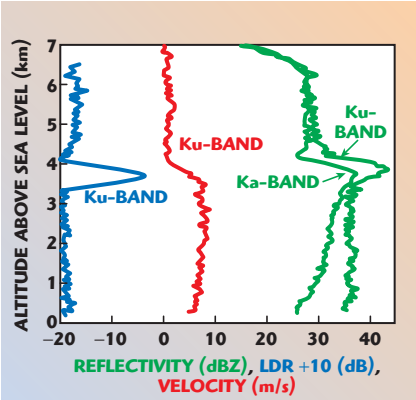

▲ *Fig. 10 Dual-frequency reflectivity, Doppler and LDR profiles in Hurricane Humberto (10 dB has been added to LDR for plotting purposes).*

tude. ***Figure 10*** shows a vertical profile from the same data. The data are presented as a function of altitude and have not been corrected for attenuation. The much larger attenuation at 35 GHz can readily be seen in this case, especially near the surface. This differential attenuation between the two frequencies can be used in retrieving the rain rate. Also shown is the Ku-band Doppler and linear depolarization ratio (LDR), which is the ratio of cross-polarization to co-polarized backscatter. At altitudes above 4 km the particles are ice and fall slowly. Below 4 km, the particles melt and collapse into rain drops with much larger fall speeds, as seen in the Doppler, which increases from approximately 1 m/s at 5 km altitude to 9 m/s at 3 km altitude. The LDR at 4 km altitude becomes enhanced as the irregularly-shaped ice particles become covered with water; note that 10 dB has been added for plotting purposes. The peak LDR at 3.8 km is approximately –14 dB, caused by scattering from partially melted, irregularly shaped ice particles, the so-called bright-band region.[1,7,9] This also causes the strong signal in the co-polarized reflectivity, especially at 13.4 GHz.

CONCLUSION

This article has described an advanced airborne precipitation radar designed to demonstrate technology that can be used by the second generation of spaceborne precipitation radars. Key features of the system include an extremely compact LO/IF module which supports Ku-band and Ka-band transmission at one polarization and reception at two polarizations, allowing co-polarized and cross-polarized backscatter from rainfall to be measured simultaneously. Another innovation is the use of FPGAs for real-time digital filtering, pulse compression and averaging. Test results in clear air have characterized the system performance. The measurements in precipitation will be used for retrieving rain rates to provide improved understanding of rainfall. ■

ACKNOWLEDGMENT

The research described here was carried out at the Jet Propulsion Laboratory, California Institute of Technology, under contract with the National Aeronautics and Space Administration (NASA). The authors would like to thank Dr. L. Li (data processing), Z. Hussein (antenna design/testing) and the entire APR-2 CAMEX-4 team. Support from the NASA Earth Sciences Enterprise Instrument Incubator Program and Convection and Moisture Experiment is gratefully acknowledged.

References

1. D. Atlas, Ed., *Radar in Meteorology*, American Meteorological Society, Boston, MA 1990.
2. T. Kozu, et al., "Development of Precipitation Radar Onboard the Tropical Rainfall Measuring Mission (TRMM) Satellite," *IEEE Transactions Geoscience and Remote Sensing*, Vol. 39, 2001, pp. 102–116.
3. S. Tanelli, E. Im, S.L. Durden, L. Facheris and D. Guili, "The Effects of Nonuniform Beam Filling on Vertical Rainfall Velocity Measurements with Spaceborne Doppler Radar," *Journal of Atmospheric Oceanic Technology*, Vol. 19, July 2002, pp. 1019–1034.
4. P. Amayenc, J.P. Diguet, M. Marzoug and T. Tani, "A Class of Single- and Dual-frequency Algorithms for Rain Rate Profiling from a Spaceborne Radar – Part II: Tests for Airborne Radar Measurements," *Journal of Atmospheric Oceanic Technology*, Vol. 13, 1996, pp. 142–164.
5. R. Meneghini, J.A. Jones and L.H. Gesell, "Analysis of a Dual-wavelength Surface Reference Radar Technique," *IEEE Transactions on Geoscience and Remote Sensing*, Vol. 25, 1987, pp. 456–471.
6. E. Im, et al., "System Concept for Next-generation Spaceborne Precipitation Radars," Proceedings of IEEE Aerospace 2000 Symposium, Big Sky, MT.
7. R. Doviak and D.S. Zrnic, *Doppler Radar and Weather Observations*, Second Edition, Academic Press, San Diego, CA 1993.
8. C.E. Cook and M. Bernfield, *Radar Signals: An Introduction to Theory and Application*, Academic Press, New York, NY 1967.
9. R. Meneghini and T. Kozu, *Spaceborne Weather Radar*, Artech House Inc., Norwood, MA 1990.
10. S.L. Durden, E. Im, F.K. Li, W. Ricketts, A. Tanner and W. Wilson, "ARMAR: An Airborne Rain Mapping Radar," *Journal of Atmospheric Oceanic Technology*, Vol. 11, No. 3, 1994, pp. 727–737.